

## Article

# Effect of Ca and P on the Size and Morphology of Eutectic Mg<sub>2</sub>Si in High-Purity Al-Mg-Si Alloys

Muhammad Zarif <sup>1</sup>, Ivo Spacil <sup>1</sup> , Thomas Pabel <sup>2</sup>, Peter Schumacher <sup>1,2</sup> and Jiehua Li <sup>1,\*</sup><sup>1</sup> Institute of Casting Research, Department of Metallurgy, Montanuniversität Leoben, A-8700 Leoben, Austria<sup>2</sup> Austrian Foundry Research Institute, A-8700 Leoben, Austria

\* Correspondence: jiehua.li@unileoben.ac.at

**Abstract:** Controlling the size and morphology of primary and eutectic Mg<sub>2</sub>Si phase via modification and refinement (i.e., Ca and P addition) in Al-Mg<sub>2</sub>Si-based alloys containing higher percentages of Si and Mg is of great necessity to ensure their high performance. The present investigation is mainly aimed to elucidate the effect of Ca and P on the nucleation and growth pattern of eutectic Mg<sub>2</sub>Si in high-purity Al-13.1 wt.% Mg<sub>2</sub>Si near-eutectic alloys with and without the additions of P and Ca. It was found that purity levels of raw starting materials exert a significant influence on the size and morphology of the near-binary eutectic Al-Mg<sub>2</sub>Si. The presence of P suppresses the precipitation of ternary eutectic Al-Mg<sub>2</sub>Si-Si. The presence of low levels of Ca promotes the faceted growth of Mg<sub>2</sub>Si, while at sufficiently higher levels of Ca, Al<sub>2</sub>Si<sub>2</sub>Ca intermetallic is formed and the morphology of the Mg<sub>2</sub>Si phase is changed from fibers/or globules to blocks or plates. The current investigation is of great importance for the further development of high-performance Al-Mg<sub>2</sub>Si-based cast alloys.

**Keywords:** Al-Mg-Si alloy; eutectic Mg<sub>2</sub>Si; Ca and P additions; DSC; SEM; TEM



**Citation:** Zarif, M.; Spacil, I.; Pabel, T.; Schumacher, P.; Li, J. Effect of Ca and P on the Size and Morphology of Eutectic Mg<sub>2</sub>Si in High-Purity Al-Mg-Si Alloys. *Metals* **2023**, *13*, 784. <https://doi.org/10.3390/met13040784>

Academic Editor: Noé Cheung

Received: 28 January 2023

Revised: 3 April 2023

Accepted: 5 April 2023

Published: 17 April 2023



**Copyright:** © 2023 by the authors. Licensee MDPI, Basel, Switzerland. This article is an open access article distributed under the terms and conditions of the Creative Commons Attribution (CC BY) license (<https://creativecommons.org/licenses/by/4.0/>).

## 1. Introduction

The 6xxx (Al-Si-Mg) wrought alloys with small additions of Si (0.7–1.3 wt.%) and Mg (0.6–1.2 wt.%) under different temper designations are some of the most widely used Al alloys due to their excellent deformation ability and mechanical properties. However, for aluminum foundry alloys, approximately 90% are based on Al-Si-Mg with higher additions of Si (about 7–12 wt.%) but low levels of Mg (0.3–0.7 wt.%) due to their excellent castability and good balance between mechanical properties and costs. Eutectic Si and  $\beta$ -series precipitates (i.e., Mg<sub>2</sub>Si) formed during the ageing treatment are mainly responsible for their strengthening effects. Apart from the eutectic Si in Al-Si-based alloys, eutectic Mg<sub>2</sub>Si in Al-Mg<sub>2</sub>Si-based alloys has also been widely studied to develop new Al-Mg<sub>2</sub>Si-based alloys containing higher percentages of Si and Mg with superior mechanical properties. Al, together with Mg and Si, forms a simple binary system with quasi-eutectic occurring at ~13.1 wt.% Mg<sub>2</sub>Si. The vertical section constructed (in ternary system) through the Al-rich corner to the point demonstrates that the composition of the compound Mg<sub>2</sub>Si is quasi-binary [1,2]. The alloys located on this line form a near-eutectic binary Al-Mg<sub>2</sub>Si. It has been reported that the Mg<sub>2</sub>Si phase is an intermetallic compound, in which the ratio of Mg/Si (about 1.73) can be adjusted to form Mg<sub>2</sub>Si [3,4]. The eutectic composition of binary Al-Mg<sub>2</sub>Si alloys has been determined [1,5–7]. However, the exact eutectic composition is still not yet well established. Previous investigations [8,9] suggested that the binary eutectic composition lies on the Mg-rich side. The Al-Mg-Si ternary system has a very narrow range for a binary Al-Mg<sub>2</sub>Si eutectic. The variations of the composition outside this range cause the formation of either the ternary eutectic of Al-Mg<sub>2</sub>Si-Si or Al-Mg<sub>2</sub>Si-Mg<sub>17</sub>Al<sub>12</sub> along with binary eutectic [10], which causes the degradation of mechanical properties at high temperatures because of the fact that the ternary eutectic of Al-Mg<sub>2</sub>Si-Si or Al-Mg<sub>2</sub>Si-Mg<sub>17</sub>Al<sub>12</sub> has a lower melting temperature and thereby cannot be used at elevated

temperatures. The composition of the ternary eutectic and its freezing temperature was also determined and documented [1,6,11]. However, the freezing temperature of these ternaries is, so far, not yet well-established. It has been reported [9] that the Al-Mg<sub>2</sub>Si eutectic solidified in a non-faceted-faceted manner, in which Mg<sub>2</sub>Si is a faceted phase while Al is a non-faceted phase. It has also been reported [12], that, using Cu wedge mold, the variation of cooling rates affects the size and morphology of the primary Mg<sub>2</sub>Si and Al-Mg<sub>2</sub>Si eutectic in a hypereutectic Al-20 wt.% Mg<sub>2</sub>Si alloy. Primary Mg<sub>2</sub>Si particles with a polygonal shape and refined Al-Mg<sub>2</sub>Si eutectic cells were observed. Furthermore, increasing the additions of mischmetal (MM) reduces the size of primary Mg<sub>2</sub>Si particles and also changes the morphology of eutectic Mg<sub>2</sub>Si from flakes to fibers in situ Al-15 wt.% Mg<sub>2</sub>Si composites [13,14]. More interestingly, additions of P changed the morphology of primary Mg<sub>2</sub>Si from dendritic or equiaxed to polygonal shape and thereby reduced the size of the particles [15]. These polygonal shape particles are advantageous for both mechanical and corrosion properties [16]. Chong et al. [17] reported that the addition of TiB<sub>2</sub> particles in Al-12.67Mg-10.33Si alloy reduced the size and changed the morphology of primary Mg<sub>2</sub>Si from dendritic to polygonal shape because TiB<sub>2</sub> particles acts as nuclei for primary Mg<sub>2</sub>Si due to their small lattice mismatch of only ~5%. On this basis, it can be concluded that most of the data are available on the modification and refinement of the primary Mg<sub>2</sub>Si phase, but limited research works are available on hypo- and near-eutectic compositions. The effect of P additions on commercial-purity Al-Mg-Si near-eutectic alloys has been reported by Pabel et al. [18,19]. The additions of P in commercial-purity Al-Mg-Si near-eutectic alloys change the morphology of the eutectic Mg<sub>2</sub>Si phase from lamellar to globular and remarkably enhanced the breaking strength of the alloy. It should be noted that although a detailed investigation on the effect of purity levels and P additions on eutectic Si in Al-Si alloys has been reported [20,21], but the effect of P additions on eutectic Mg<sub>2</sub>Si phase in high-purity Al-Mg-Si near-eutectic alloys (in contrast to commercial-purity Al-Mg-Si near-eutectic alloys [18,19]) is still lacking. In terms of Ca addition, Moussa et al. [22] reported that the addition of 0.3 wt.% of Ca can effectively modify the morphology and refine the size of the primary Mg<sub>2</sub>Si and produced best wear properties in hypereutectic Mg-5 wt.%Si alloy. It was also proposed [23] that the addition of Ca refine the eutectic Mg<sub>2</sub>Si by the creation of Ca-based compounds which acted as nucleation sites for Al-Mg<sub>2</sub>Si eutectic in hypoeutectic Al-Mg<sub>2</sub>Si alloy. Another study [24] showed that the presence of Ca refines both the primary and eutectic Mg<sub>2</sub>Si which resulted in the improvement of tensile properties in Mg-Mg<sub>2</sub>Si composites. A literature survey suggested that the previous studies on Ca are mainly focused on the hypo and hypereutectic region. However, the effect of P and Ca on the nucleation and growth of eutectic Mg<sub>2</sub>Si is not well understood in quasi-binary Al-Mg<sub>2</sub>Si eutectics. This investigation is an attempt to further explain and clarify the effect of P and Ca on the size and morphology of near-eutectic Al-Mg<sub>2</sub>Si in a high-purity Al-Mg-Si alloy system, which is of great importance for the further development of high-performance Al-Mg<sub>2</sub>Si-based alloys.

## 2. Materials and Methods

Al-13.1 wt.% Mg<sub>2</sub>Si eutectic alloys with and without additions of P and/or Ca, were prepared using 99.999 wt.% (5N) super purity electrolytically refined Al (Hydro Aluminium High Purity GmbH, Grevenbroich, Germany) and 99.999 wt.% (5N) purity Si (Siltronic AG GmbH, Munich, Germany) and 99.93 wt.% (3N3) Mg obtained from SAG GmbH (Lend, Austria). Additions of P and Ca were made using Al-19 wt.% Cu-1.4 wt.%P and Al-10 wt.%Ca master alloy rods, respectively. It should be noted that when P was added, Cu was also added, but the possible effect of Cu on the eutectic Mg<sub>2</sub>Si phase are not included here. The alloys were first prepared by melting Al and Si together in a clay-bonded graphite crucible in an electric resistance furnace. The crucible was coated from the inside by ceramic material (BN) to avoid any possible reaction between the molten material and the crucible. The calculated amount of Mg was subsequently added. All alloys were gravity die cast in a specially designed permanent cast iron mold at a temperature of

~720 °C. The mold temperature was kept at 350 °C. The melt temperature was measured using a portable K-type Chromel-Alumel thermocouple connected to a digital meter, which is able to measure temperatures up to 1300 °C. Graphite spray was applied inside the mold prior to pouring to increase heat transfer through mold wall and facilitate the removal of the cast from the mold. A filter was placed at the location shown in Figure 1a to reduce the effect of bi-films and to ensure the smooth entrance (with a minimum turbulence) of the melt into the mold. Figure 1 shows the pictures of the permanent mold, an actual cast part and the die dimensions (unit: mm), respectively. Alloys with additions of 50, 200 and 300 ppm P levels were also manufactured using the same procedures. Quantitative chemical analysis was obtained from OES-spark analysis whilst the trace P content was measured using glow discharge mass spectroscopy (GDMS) (SHIVA Technologies, EAG Lab., Toulouse, France). The measured compositions of all manufactured alloys are listed in Table 1. In addition, a high-purity Al-13.1 wt.% Mg<sub>2</sub>Si eutectic alloy containing 500 ppm Ca (only 0.4 ppm P) was also prepared by using the same experimental procedure in order to elucidate the effect of high Ca addition levels on the eutectic Mg<sub>2</sub>Si phase (also listed in Table 1).

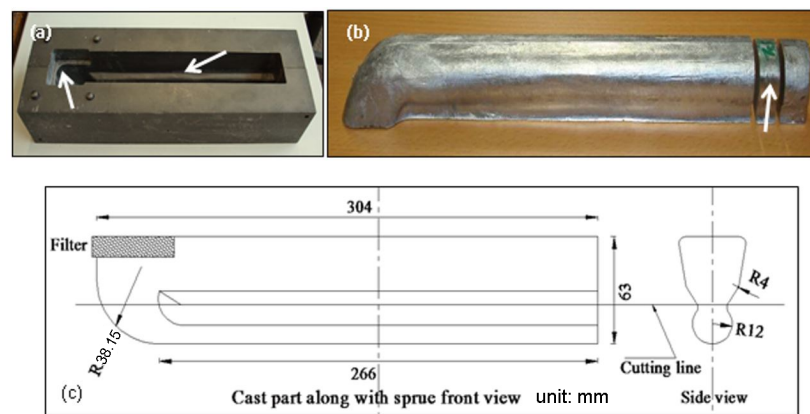


**Figure 1.** (a) Cast iron permanent mold used for casting, (b) photograph of actual cast part and (c) sketch showing the die dimensions (unit: mm). The white arrows from left to right indicate the provision in the die for the filter placement, casting cavity and the cutting of samples for microstructural characterization, respectively.

**Table 1.** Measured composition of five alloys manufactured for this investigation.

No.	Mg wt.%	Si wt.%	P (ppm)	Fe (ppm)	Ca (ppm)	Cu wt.%	Cr (ppm)	Ni (ppm)	Ti (ppm)	Al
1	8.61	4.58	0.4	<5	27	<1	<3	<4	<4	Bal.
2	8.45	4.60	50	35	8	0.045	<3	<4	<4	Bal.
3	8.64	4.54	200	40	6	0.273	<3	<4	<4	Bal.
4	8.45	4.60	300	44	6	0.366	<3	<4	<4	Bal.
5	8.50	4.60	0.4	35	500	<1	<3	<4	<4	Bal.

Scheil simulation using Thermo-Calc software (2022b, Stockholm, Sweden) with a TTAL5 database was performed to predict the phases formed during solidification. Their formation temperatures and relevant mole or weight fractions of all solid phases or each phase were also calculated. A Quik-Cup obtained from Heraeus Electro-nite GmbH (Bitterfeld-wolfen, Germany) was employed to analyze the thermal response of the alloys. For DSC analysis, samples were machined in the forms of small discs and with weights of ~50 mg. Samples were heated from 350 °C to 620 °C at a heating rate of 20 °C/min in a power-compensated PerkinElmer (Waltham, MA, USA) diamond DSC apparatus. Samples were held at this temperature (620 °C) for 10 min to ensure the homogenization of 620 °C and then cooled from 620 °C to 350 °C with the same cooling rate (20 °C/min.)

Sample preparation for microstructure characterization followed the standard methods, including grinding and polishing. For optical microscopy, ZEISS Imager AXIO was used, while SEM analysis was performed on a FEI QUANTA 200 equipped with an EDX (Oxford Instruments INCA x-sight, Abingdon, UK) system. For image analysis, a NIS elements BR 3.0 SP3 Hotfix 4 build 472 basic research software (NIKON, Japan) was employed. The measurement of the distribution and shape factor of  $Mg_2Si$  was carried out with at least three different micrographs and a minimum of 50 readings were taken each time. The obtained results can be expected to be typical and reliable. In order to examine the three-dimensional (3D) morphology of eutectic  $Mg_2Si$ , samples were deeply etched using 30% NaOH solution at a temperature of 60 °C for 10 min [25]. Thin foil specimens for TEM investigations were prepared by a Model 691 Gatan PIPS™ (Precision Ion Polishing System, Gatan, Pleasanton, CA, USA) with an angle of 4° and a voltage of 4 KV. TEM was performed using a Philips CM12 (Philips, Eindhoven, The Netherlands) operated at 120 KV and an image-corrected JEOL-2100 (JEOL Ltd., Tokyo, Japan) operated at 200 KV.

### 3. Results

#### 3.1. Scheil Simulation

Scheil simulation using Thermo-Calc software with a TTAL5 database was performed by adding Mg = 8.6 wt.%, Si = 4.5 wt.% and the remaining aluminum, respectively. The simulation was used to predict the formation temperature of eutectic, weight fraction and solidification range of the solid phases evolved during solidification. Figure 2 illustrates the mole fraction of solid phases and weight fraction of  $Mg_2Si$  phase in near-eutectic Al-13.1 wt.%  $Mg_2Si$  alloy without adding any other chemical elements. The liquidus and eutectic temperatures of the manufactured alloys were predicted to be ~598 °C and ~594 °C, respectively, as shown in Figure 2a. The labeled numbers 1–4 show the solidification path of the phases. The presence of the Si phase at the end of solidification along with Al and  $Mg_2Si$  was also predicted, as shown in Figure 2b. The black curve in Figure 2a was predicted under the equilibrium conditions.

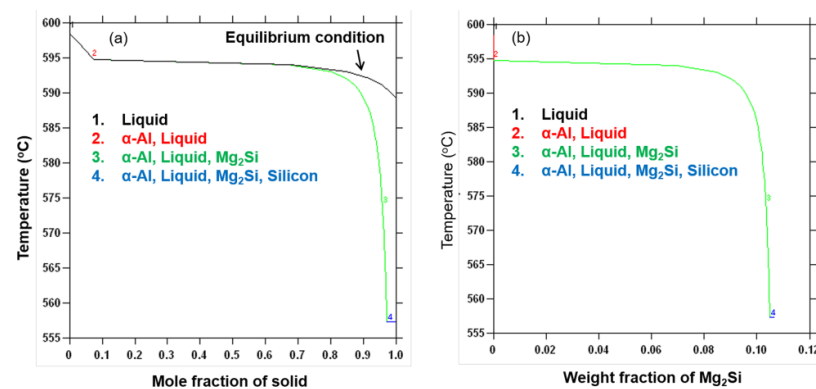


**Figure 2.** (a) Mole fractions of all solids formed during the solidification of a near-eutectic Al-13.1 wt.%  $Mg_2Si$  alloy and (b) the weight fraction of the  $Mg_2Si$  phase in an Al-13.1 wt.%  $Mg_2Si$  alloy without the addition of chemical elements. The labeled number indicates the solidification range of the solid phases. The simulation is based on a Scheil model. The black curve in (a) was predicted under equilibrium conditions.

#### 3.2. Thermal Analysis

Figure 3a shows the cooling curve (black) of the Al-13.1wt.%  $Mg_2Si$  near-eutectic alloys without the addition of chemical elements. Two distinct peaks can be observed on the superimposed 1st derivative  $dT/dt$  curve (blue). The first peak corresponds to the nucleation of the Al- $Mg_2Si$  eutectic (indicated by a sharp increase in the 1st derivative  $dT/dt$  curve), while the second peak signifies the nucleation of ternary eutectic Al- $Mg_2Si$ -Si at a temperature of ~548 °C. Experimentally, the liquidus temperature of the alloy was measured as ~600 °C (close to the calculated value (598 °C) by Thermo-Calc) and the

eutectic temperature was measured as  $\sim 594^\circ\text{C}$  (the same as the calculated value ( $594^\circ\text{C}$ ) by Thermo-Calc). This indicates that the experimental and simulation results are in a good agreement. Figure 3b shows the DSC solidification exotherms for the Al-Mg<sub>2</sub>Si near-eutectic alloy without the addition of chemical elements. The first sharp exotherm A represents the nucleation of Al-Mg<sub>2</sub>Si eutectic cells and a smaller exotherm manifests the nucleation of ternary eutectic (i.e., Al-Mg<sub>2</sub>Si-Si) with the nucleation temperature onset of  $\sim 548^\circ\text{C}$ . It should be noted that the exotherm A is not sharp, which can be attributed to the higher sample masses ( $\sim 50$  mg) employed in the DSC pan in order to clearly observe the exotherm B.

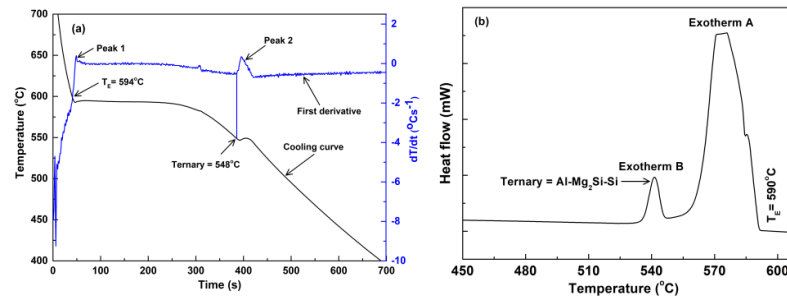


**Figure 3.** (a) Cooling curve (black) and superimposed 1st derivative  $dT/dt$  (blue) curve, and (b) DSC exotherms observed for the Al-13.1 wt.% Mg<sub>2</sub>Si alloy without the addition of chemical elements.

P content in the Al-13.1 wt.% Mg<sub>2</sub>Si alloy without the addition of chemical elements was measured as 0.40 ppm by using the GDMS technique. Figure 4a,b shows the cooling curves (black) for the alloys containing 200 and 300 ppm P, respectively, with the superimposed 1st derivative  $dT/dt$  curves (blue). In both cases, only one sharp increase in the 1st derivative  $dT/dt$  curve (i.e., the nucleation of the Al-Mg<sub>2</sub>Si eutectic) was observed, while no further variations in cooling rate were recorded. Figure 4c shows the DSC solidification exotherms of Al-Mg<sub>2</sub>Si alloys with different addition levels of P. In the first thermogram (with 50 ppm P content), a small ternary eutectic peak was evident, while in thermograms 2 and 3, no other peak was apparent except the large exotherm A. This may be due to the fact that the addition of P restrains the nucleation of the ternary Al-Mg<sub>2</sub>Si-Si eutectic.

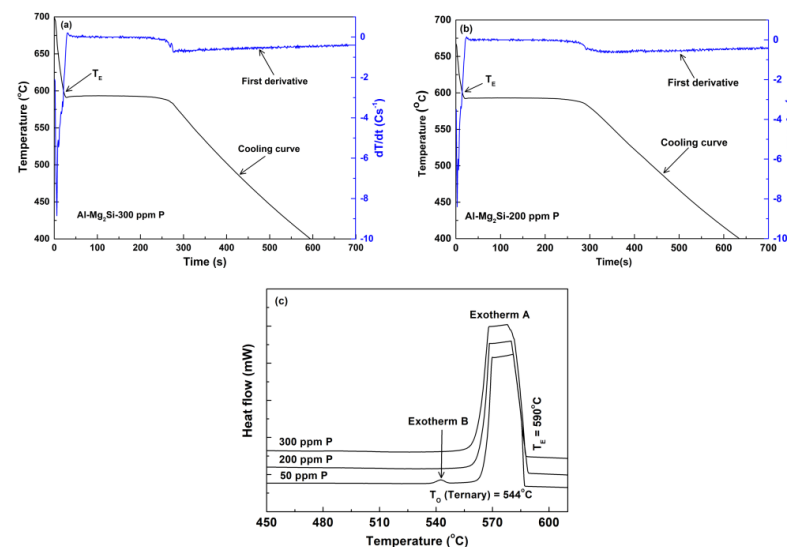


**Figure 4.** (a,b) Cooling curves for the Al-Mg<sub>2</sub>Si-200 ppm P and the Al-Mg<sub>2</sub>Si-300 ppm P eutectic alloys, respectively, and (c) the DSC traces of the Al-Mg<sub>2</sub>Si eutectic alloys with different addition levels of P cooled from  $620^\circ\text{C}$  to  $350^\circ\text{C}$  with a cooling rate of  $20^\circ\text{C}/\text{min}$  after holding at  $620^\circ\text{C}$  for 10 min.

### 3.3. Microstructural Characterization

Figure 5 shows the optical micrograph of the Al-13.1 wt.% Mg<sub>2</sub>Si near-eutectic without any addition at lower and higher magnifications when the mold was heated to 350 °C prior to pouring. The microstructure mainly consists of fine Al-Mg<sub>2</sub>Si eutectic cells. Mg<sub>2</sub>Si, with fibrous or cylindrical shape, along with visible irregular and dog bone-shaped morphology, can be seen in Figure 5d at a higher magnification. Figure 6 shows the micrographs of fine Al-Mg<sub>2</sub>Si eutectic grains at a mold temperature of 350 °C. The detailed analysis of the micrographs was performed using image analysis software (NIS elements BR 3.0 SP3 Hotfix 4 build 472). Various geometrical features of the Mg<sub>2</sub>Si phase were calculated, including area (μm<sup>2</sup>), perimeter (μm), equivalent diameter (μm) and phase count. It should be noted that mean values of the number of Mg<sub>2</sub>Si fibers in the selected region of interest (ROI), i.e., 10 × 10 μm<sup>2</sup> (see Figure 6b), are 110, while average equivalent diameter [26,27] was approximately ~0.3732 μm when the mold temperature was kept at 350 °C. Figure 6d shows a ternary eutectic which formed in the vicinity of or at the eutectic cell boundaries in the alloy containing only 0.4 ppm P. Figure 7a shows an SEM backscattered (BS) image in which three phases (i.e., Al, Mg<sub>2</sub>Si and Si) can be distinguished by color contrast, as indicated by arrows on the micrograph. Figure 7b shows corresponding elemental maps from the selected region. The color contrast illustrates the presence of Al, Mg and Si, respectively. Figure 8 shows optical and SEM micrographs for the alloy containing 300 ppm P and no ternary eutectic was apparent in the vicinity of or at the eutectic cell boundaries; however, a few primary Mg<sub>2</sub>Si particles with a regular shape were observed. Figure 9 shows deep-etched SEM BS images of the Al-13.1 wt.% Mg<sub>2</sub>Si-300 ppm P alloy. The 3D fibrous morphology of Mg<sub>2</sub>Si is visible on both micrographs along with a few polygonal-shaped Mg<sub>2</sub>Si particles. Figure 10 shows a SEM secondary electron (SE) image taken from a deeply etched sample and an EDX spectrum taken from the selected point, which confirms the Mg<sub>2</sub>Si phase composition. In order to further elucidate the shape of the eutectic Mg<sub>2</sub>Si phase, Figure 11a–c illustrates the bright-field TEM image and the corresponding selected area diffraction pattern of the Al-13.1 wt.% Mg<sub>2</sub>Si alloy. The faceted Mg<sub>2</sub>Si phase can easily be identified on the micrograph.

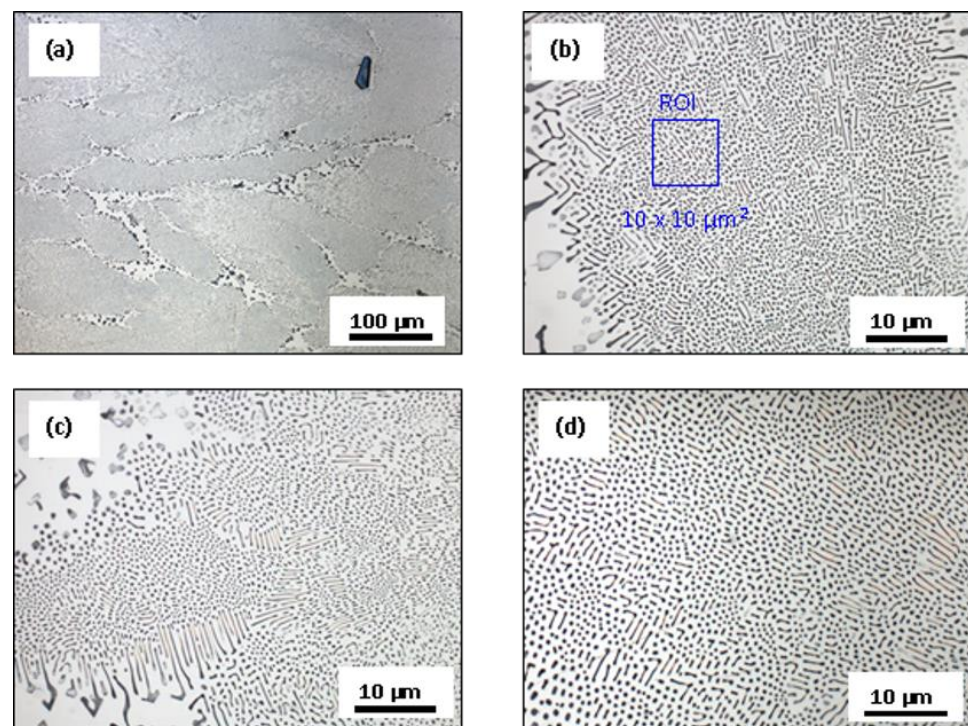


**Figure 5.** Microstructure of the Al-13.1 wt.% Mg<sub>2</sub>Si near-eutectic alloy at a 350 °C mold temperature, (a) at a lower magnification and (b–d) at higher magnifications prepared using ultra-pure materials.

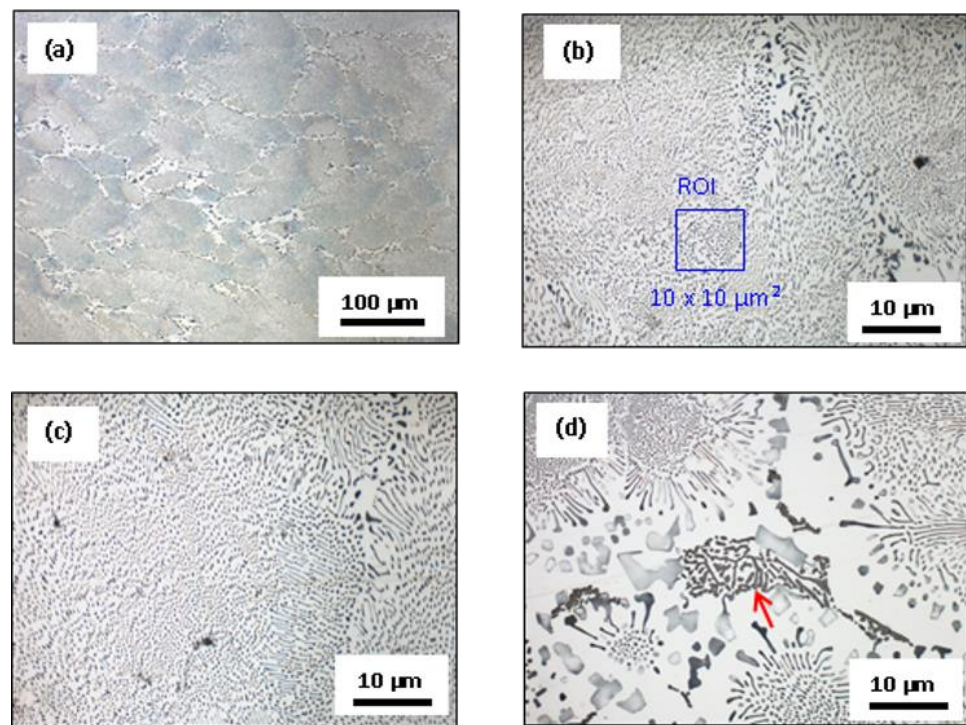


**Figure 6.** Microstructure of the Al-13.1 wt.% Mg<sub>2</sub>Si eutectic at a 350 °C mold temperature, (a) at a lower magnification and (b–d) at higher magnifications. The red arrow indicates the presence of a ternary eutectic.

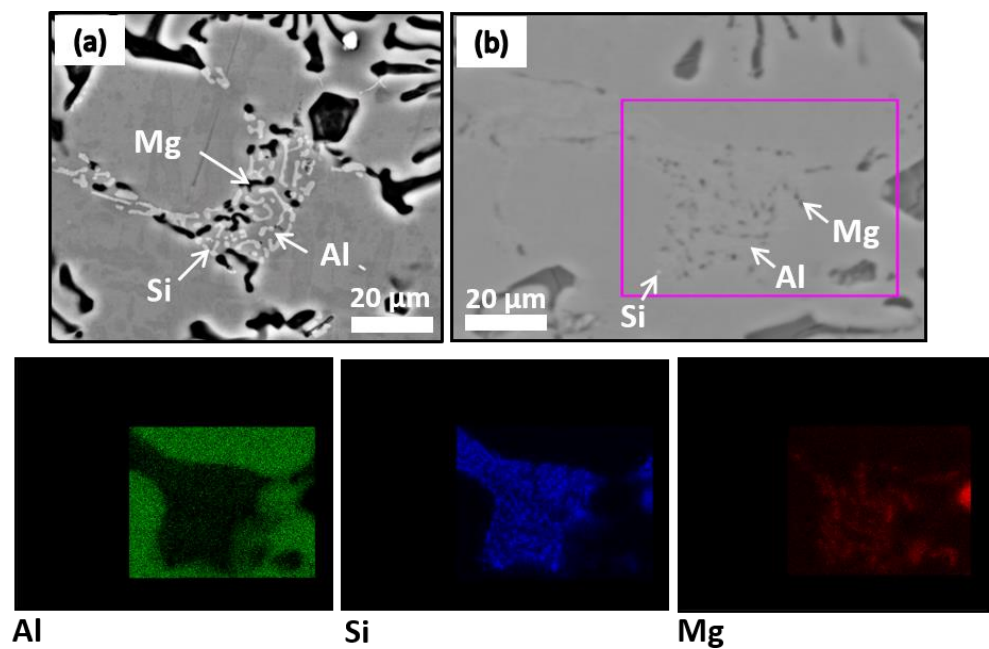


**Figure 7.** (a,b) SEM backscattered (BS) image and corresponding EDS elemental maps from the selected region for the Al-13.1 wt.% Mg<sub>2</sub>Si alloy showing the presence of Al, Mg and Si.

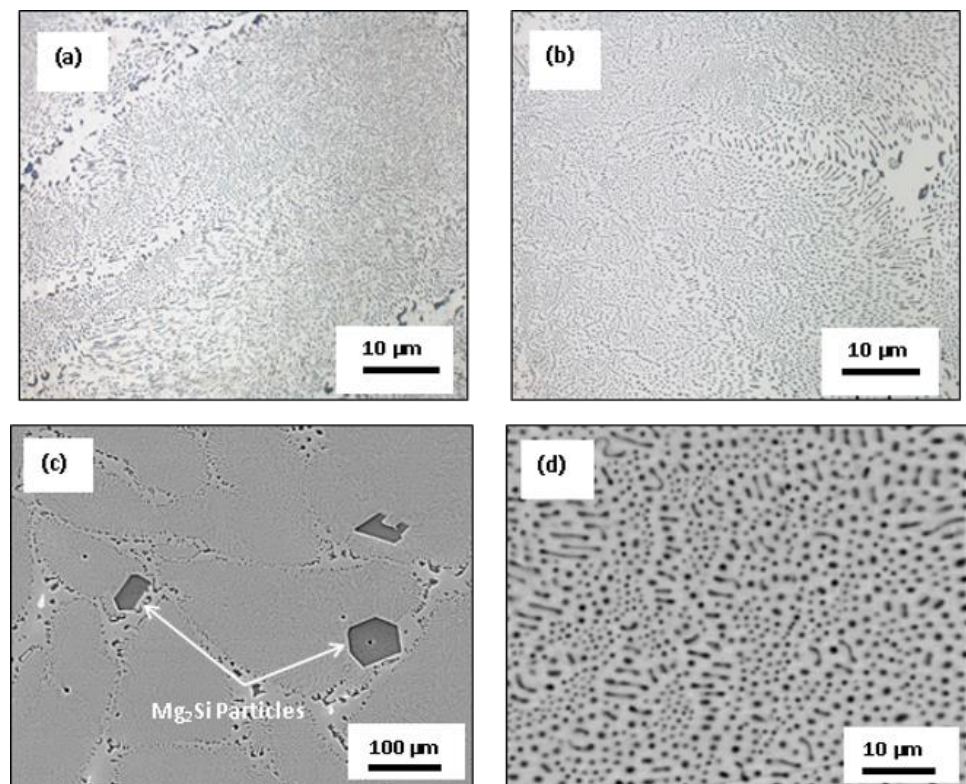


**Figure 8.** (a,b) Optical micrographs and (c,d) SEM BS images of the Al-13.1 wt.%  $Mg_2Si$ -300 ppm P alloy with a mold temperature of 350 °C.

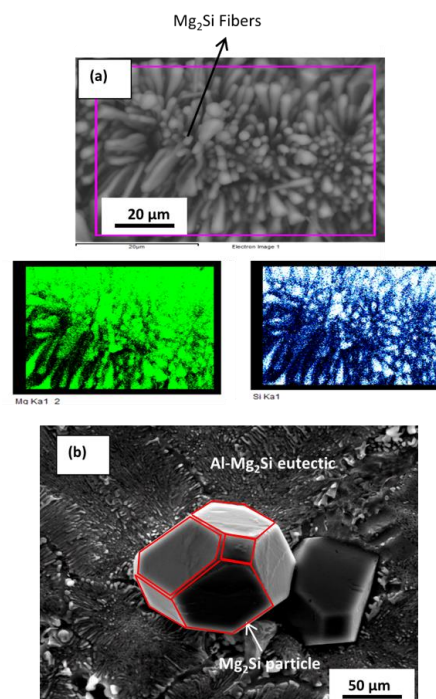


**Figure 9.** (a) SEM BS image taken from a deep-etched sample and the corresponding EDS elemental maps from the selected region and (b) a deep-etched sample showing a primary polygonal-shaped  $Mg_2Si$  particle for the Al-13.1 wt.%  $Mg_2Si$ -300 ppm P alloy. White arrows indicate squares and a hexagons structure, which is identical to the geometrically shaped tetrakaidecahedron.

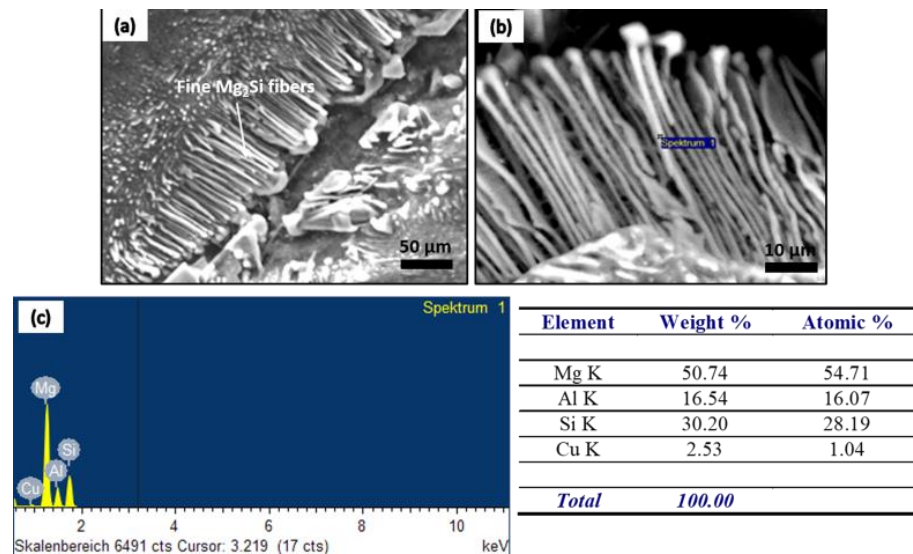


**Figure 10.** (a,b) SEM SE images taken from the deep-etched sample, which confirm the fibrous morphology of  $Mg_2Si$  in the Al-13.1 wt.%  $Mg_2Si$ -200 ppm P alloy along with (c) the EDS spectrum of elements from the selected point, as marked in (b).

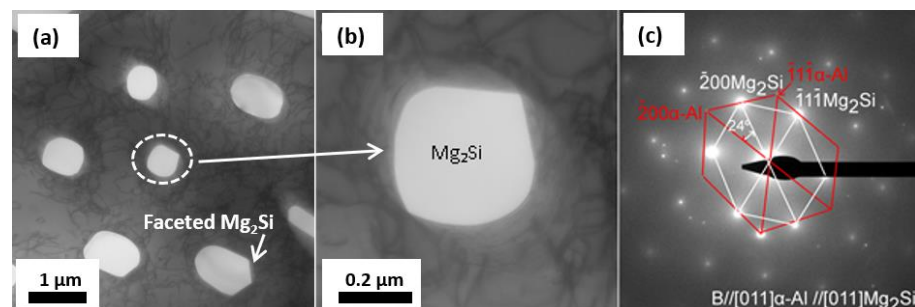


**Figure 11.** (a) bright-field TEM image showing the Al- $Mg_2Si$  eutectic at a lower magnification, (b) shows the faceted eutectic  $Mg_2Si$  globules with a diameter of  $\sim 0.4 \mu m$  at a higher magnification and (c) the corresponding selected area diffraction pattern taken parallel to the electron beam direction of  $[011]_{\alpha-Al}$ .

In addition, in order to elucidate the effect of Ca on the shape of the eutectic  $Mg_2Si$  phase, Figure 12a shows the presence of the  $Al_2Si_2Ca$  intermetallic in the Al-Mg-Si alloy system containing 500 ppm Ca. Figure 12b–e shows the corresponding elemental maps, while Figure 12f represents the EDS spectrum taken from the location, as shown in Figure 12a. It should be noted that, at the higher levels of Ca, the morphology of  $Mg_2Si$  is changed from fibers or globules to a block/or plate. Figure 12g shows a schematic diagram, which indicates the presence of  $Al_2Si_2Ca$  at the growing interfaces of the  $Mg_2Si$  phase. Furthermore, Figure 13 shows the plate-shaped  $Mg_2Si$  phase. No Ca-rich layer was observed along the plate-shaped  $Mg_2Si$  in the  $[011]$  zone axis within the resolution in the present investigation. Figure 14 shows the globular-shaped  $Mg_2Si$  phase. No Ca-rich layer was observed along the globular-shaped  $Mg_2Si$  in  $[011]$  zone axis within the resolution in the present investigation. A detailed analysis concerning thermal analysis, DSC and microstructure characterization is discussed below.

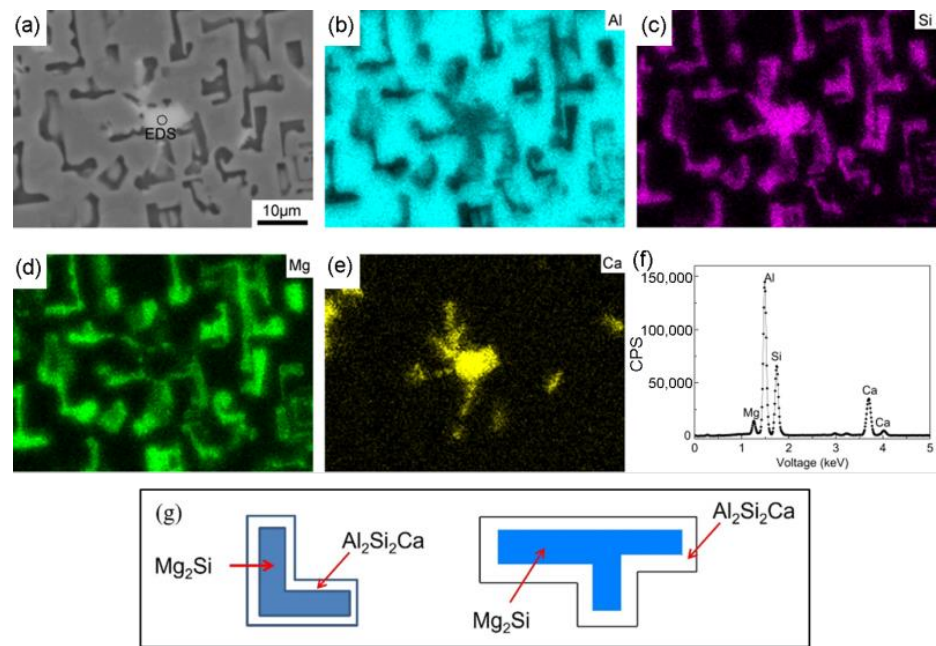


**Figure 12.** (a) The presence of  $\text{Al}_2\text{Si}_2\text{Ca}$  intermetallic in the Al-Mg-Si alloy system containing 500 ppm Ca. (b–e) The corresponding EDS elemental maps, while (f) the EDS taken from the location, as shown in (a). It should be noted that, at the higher levels of Ca, the morphology of  $\text{Mg}_2\text{Si}$  is changed from fibers or globules to a block/or plate. (g) A schematic diagram, showing the presence of  $\text{Al}_2\text{Si}_2\text{Ca}$  on the growing interfaces of the eutectic  $\text{Mg}_2\text{Si}$  phase.

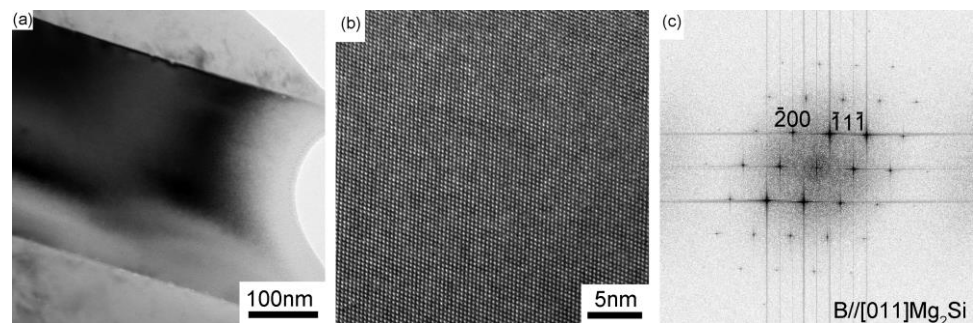


**Figure 13.** (a) Bright field TEM image, (b) HRTEM image and (c) the fast Fourier transform (FFT) of the plate-shaped  $\text{Mg}_2\text{Si}$  phase. No Ca-rich layer was observed along the plate-shaped  $\text{Mg}_2\text{Si}$  in the  $[011]_{\text{Mg}_2\text{Si}}$  zone axis within the resolution in the present investigation.

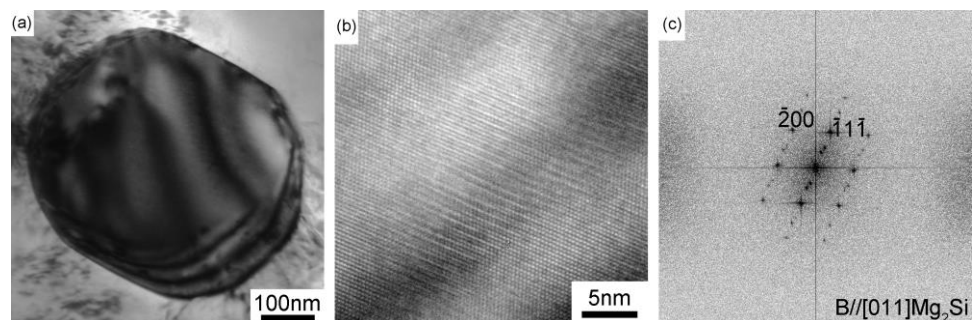


**Figure 14.** (a) Bright field TEM image, (b) HRTEM image and (c) FFT of the globular-shape  $\text{Mg}_2\text{Si}$  phase. No Ca-rich layer was observed along the globular-shaped  $\text{Mg}_2\text{Si}$  in the  $[011]_{\text{Mg}_2\text{Si}}$  zone axis within the resolution in the present investigation.

## 4. Discussion

### 4.1. Microstructure without and with Additions of Ca

The microstructure of the Al-13.1 wt.% Mg<sub>2</sub>Si near-eutectic consists of very fine eutectic grains (see Figures 5 and 6). Two-dimensional (2D) fine Mg<sub>2</sub>Si globules should be fibers in 3D with a short length. For the formation of the Mg<sub>2</sub>Si compound, the solidification theory suggests that the solute redistribution during solidification increases the local concentration of both Si and Mg in the melt, which leads to the formation of intermetallic Mg<sub>2</sub>Si. This occurs because there is a strong chemical affinity between Si and Mg. The nucleation and growth mechanism for a high-purity Al-13.1 wt.% Mg<sub>2</sub>Si near-eutectic is proposed below, in spite of a lack of strong experimental support.

#### 4.1.1. Nucleation Mechanism

The nucleation during solidification will always be aided by the presence of inherent impurities in the melt. However, the alloys in the present investigation were manufactured using high-purity materials; furthermore, in-mold filtration was employed to minimize the effect of oxides. In this scenario, the presence of fine eutectic grains in high-purity melts can be explained as follows: firstly, during an initial eutectic reaction, Al, as the major phase, will nucleate first at some unknown substrate or independently (homogeneously at a larger undercooling), which then acts as a nucleating agent for Mg<sub>2</sub>Si. This occurred simultaneously in eutectic cells, initiating in melt volume at multiple locations. In each eutectic cell, a so-called decoupled growth then proceeds separately until it terminates at the cell boundaries with the creation of irregular and faceted Mg<sub>2</sub>Si. Secondly, the independent or homogeneous nucleation of both Al and Mg<sub>2</sub>Si occurred at a high undercooling at multiple locations in a given melt volume, and eutectic will then grow in a decoupled manner. Thus, a globule and fine structure may form due to the absence of favorable nucleation sites, but the growth proceeds extremely slowly. The proposed nucleation sequence is shown schematically in Figure 15.

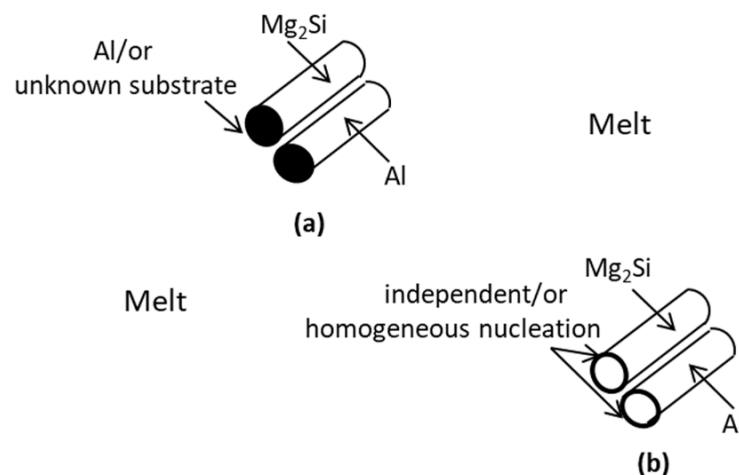


**Figure 15.** (a) Proposed nucleation sequence. Mg<sub>2</sub>Si nucleates on Al/or some unknown substrate whilst Al is nucleating independently or homogeneously, and a decoupled growth occurs at a higher undercooling. (b) Both phases nucleate independently at a higher undercooling point and then the eutectic grows in a decoupled manner. This can occur simultaneously at multiple locations in the melt volume, which finally leads to the formation of separate eutectic cells.

As discussed above, it can be concluded that impurities present in the raw starting materials may have a significant influence on the morphology, size and distribution of Mg<sub>2</sub>Si in the Al-Mg<sub>2</sub>Si near-eutectic alloys. However, the exact nucleation and growth mechanisms involved remain unclear and still need further investigations. DSC traces and thermal analysis (see Figure 3a,b) also confirm the presence of ternary eutectic. The freezing point of ternary eutectic was found to be 548 °C (apparent on DSC traces), which

is less than in previous findings [6,11]. The recorded lower freezing temperature for ternary eutectic nucleation might be due to the use of ultra-pure materials for alloy preparation and thus an absence of favorable nucleation sites. However, the exact composition of the ternary eutectic was not determined in the present investigation. The Al-Mg-Si ternary system has a narrow range for the binary Al-Mg<sub>2</sub>Si eutectic [10]. The presence of a ternary eutectic (i.e., Al-Mg<sub>2</sub>Si-Si (see Figure 6d) at the eutectic cell boundaries might suggest that there is still a slight variation in the composition of the selected alloy, i.e., Al-13.1 wt.% Mg<sub>2</sub>Si. Due to this, the excess Si is available in the melt at the end of solidification, alongside the required Si for the formation of Mg<sub>2</sub>Si, and thus nucleates and grows simultaneously to Al and Mg<sub>2</sub>Si.

#### 4.1.2. Growth Mechanism

In high-purity Al-Mg-Si near-eutectics, the presence of fibrous Mg<sub>2</sub>Si suggests that the growth of the Mg<sub>2</sub>Si phase is isotropic. A similar growth pattern of Si was also observed in Al-Si hypoeutectic alloys with the addition of impurity elements, such as Sr and Na [20,21,28], which are well-known as the impurity-induced twinning mechanisms (IIT), but no inherent twins were observed in Mg<sub>2</sub>Si in the present investigation under the given growth conditions. Furthermore, at the eutectic cell boundaries, towards the end of solidification, the growth pattern of Mg<sub>2</sub>Si changes from fiber to irregular flake shapes, which can be seen clearly in deep-etched samples (Figures 9 and 10). This indicates that the growth pattern changes from a non-faceted to faceted mode (growth takes place along certain crystallographic directions). Jackson [29–31] proposed a relationship to distinguish between faceted and non-faceted materials in terms of a factor  $\alpha$ , which can be expressed as:

$$\alpha = \left( \frac{\Delta S_m}{R_g} \right) \left( \frac{CN_s}{CN_I} \right) \quad (1)$$

where  $\Delta S_m$  is the entropy of fusion in J/mol and  $R_g$  is the ideal gas constant measured in J/mol.K.  $CN_s$  is the surface coordination number,  $CN_I$  is the internal coordination number. Surprisingly, for Mg<sub>2</sub>Si (nucleating at a high undercooling),  $\alpha$  is less than 2, and for Al,  $\alpha$  is also less than 2. The calculation of  $\alpha$  factor is given in the Supplemental Materials (SI). This suggests that the eutectic will grow in a non-faceted/non-faceted manner (regular eutectic). However, TEM image (Figure 11) confirms the presence of a faceted eutectic Mg<sub>2</sub>Si phase. A question that arises here concerns why the growth pattern of Mg<sub>2</sub>Si changes from the non-faceted to the faceted mode. It should be noted that a noticeable amount of Ca (see Table 1) is still present, although the alloys were prepared using high-purity Al. The key point is that during the electrolytic refining of aluminum by the so-called “three-layer method”, Ca is added into the electrolyte as CaF<sub>2</sub> (calcium fluorite) to increase its conductivity. From there, Ca is deposited at the cathode along with Al [32] and became an impurity within high-purity Al. The presence of the Ca plays an important role here, which may change the growth pattern, as discussed below. In the first case, when Ca is present in small quantities, the rejection of Ca (since Ca has no solid solubility [33] in Al) ahead of the growing fronts of Mg<sub>2</sub>Si may produce a fine layer of either Al<sub>2</sub>Si<sub>2</sub>Ca, Ca<sub>2</sub>Si or Ca<sub>x</sub>Mg<sub>y</sub>Si (x and y describe the possibilities of the formation of different stoichiometric compounds) intermetallic [29,34], and this Ca-rich layer might act as a precursor to increasing the Jackson  $\alpha$  factor (i.e.,  $\alpha > 2$ ), which is just sufficient to force the microscopic appearance of Mg<sub>2</sub>Si from non-faceted to faceted, as shown in TEM images (Figure 11a,b). However, at this level of Ca, no Ca-rich layer was observed along the fibers and plates of Mg<sub>2</sub>Si. In the second case, when Ca is present in large quantities, the morphology of eutectic Mg<sub>2</sub>Si is changed from a fiber to a plate and/or block, as shown in Figure 12a. Ca is proposed to play a dual role. Firstly, instead of forming a fine Ca-rich layer at growing interfaces, it may substitute inside Mg<sub>2</sub>Si as (Ca, Mg)<sub>2</sub>Si and increase its entropy of fusion, which alters the growth pattern of Mg<sub>2</sub>Si from non-faceted to faceted. The argument is based upon the EDS map of Ca (Figure 12e), in which Ca and Mg overlap. It is important to note that the entropy of the fusion of a compound is related to the degree of disorder in the system, which can be affected by

changes in the composition or structure of the compound. In the case of  $(\text{Mg}, \text{Ca})_2\text{Si}$ , if Ca replaces Mg in  $\text{Mg}_2\text{Si}$  (Ca distribution is evident in  $\text{Mg}_2\text{Si}$  crystal, see Figure 12), the degree of disorder in the system may increase. This is because of the fact that Ca and Mg have different ionic radii and chemical properties, which can lead to changes in the crystal structure of the compound. However, it should also be noted that the exact magnitude of the increase in the entropy of fusion depends upon the amount of Ca that is incorporated into the  $\text{Mg}_2\text{Si}$  lattice and the resulting changes in the crystal structure. Secondly, the formation of the  $\text{Al}_2\text{Si}_2\text{Ca}$  intermetallic, at sufficiently higher levels of Ca, appears to nucleate on  $\text{Mg}_2\text{Si}$  and forces the eutectic  $\text{Mg}_2\text{Si}$  to grow as blocks and/or plates, as shown in the SEM image Figure 12a and schematically in Figure 12g. The EDS shown in Figure 12f validates the appearance of  $\text{Al}_2\text{Si}_2\text{Ca}$ . Moreover, no Ca-rich layer was observed along both plate and fiber shape  $\text{Mg}_2\text{Si}$  in the Al-Mg-Si alloy containing 500 ppm Ca. The TEM images (Figure 13a–c), taken by tilting toward the zone axis [011], confirm the absence of a Ca-rich layer along the plate shape  $\text{Mg}_2\text{Si}$  within the resolution in the present investigation. Similarly, the TEM images (Figure 14a–c), taken by tilting toward the zone axis [011], of globular-shaped  $\text{Mg}_2\text{Si}$  also show no Ca-rich layer along the globular-shape  $\text{Mg}_2\text{Si}$  within the resolution in the present investigation. On the basis of the above evidence, it can be concluded that when Ca is present in higher quantities, it either forms a separate  $\text{Al}_2\text{Si}_2\text{Ca}$  or substitutes inside  $\text{Mg}_2\text{Si}$ .

#### 4.2. Effects of P on Nucleation and Growth of Ternary Eutectic

Cooling curves (Figure 3a) and DSC solidification thermograms (Figure 3b) revealed the presence of the ternary eutectic phase. However, with the addition of 200 ppm to 300 ppm of P, the exotherm B, which corresponds to the solidification of the ternary eutectic (i.e., Al-Mg<sub>2</sub>Si-Si), is absent. This effect of P, observed in high-purity near-eutectic Al-Mg-Si alloys, is in accordance with the previously published patent work by Pabel et al. [18] in the commercial-purity Al-13.1 wt.%  $\text{Mg}_2\text{Si}$  near-eutectic alloys. It has also been reported that additions of Li produced similar results [30], but much higher quantities (Li) are required in comparison to P. Ternary eutectic (i.e., Al-Mg<sub>2</sub>Si-Si in the present investigation) has a melting point of only ~548 °C and forms at the lateral stages of solidification and nucleates at eutectic cell boundaries. The presence of this ternary eutectic in the alloy causes the degradation of mechanical properties at high temperatures due to the fact that the ternary eutectic has a low melting temperature [10].

The suppressing action of P on the nucleation of the ternary eutectic can be explained as follows. On the one hand, if primary Al dendrites are formed during the initial decoupled eutectic reaction, they may act as nucleating substrates for AlP. This is also true for hypoeutectic Al-Si alloys, where Al is formed first at a low P content and under non-equilibrium conditions. It is well-established that the AlP compound is a potent nucleation site for Si in hypoeutectic Al-Si alloys [35–38]. Similarly, in Al-Mg<sub>2</sub>Si alloys with a low P content, some AlP may be available to nucleate excess Si. On the other hand, in the case of eutectic and hypereutectic Al-Mg<sub>2</sub>Si alloys at a higher P content, AlP formed first and then  $\text{Mg}_2\text{Si}$  nucleates directly on AlP. Ultimately, no or less (if any) AlP is available to nucleate excess Si. The remaining Si may then form an Al-Si binary eutectic or appear as free Si alone if a higher amount of Si is available. This free Si might form at the eutectic cell boundaries. Furthermore, another important aspect is the interaction between Ca and P. Thermodynamics revealed that, during solidification, the binary compound calcium phosphide, i.e.,  $1/2\text{Ca}_3\text{P}_2$  is formed preferentially, since the free enthalpy  $\Delta G_{298.15}$  of calcium phosphide  $\text{Ca}_3\text{P}_2$  is lower than the free enthalpy of AlP [39]. The reaction  $3/2\text{Ca} + 2\text{P} \rightarrow 1/2\text{Ca}_3\text{P}_2$  suggested that Ca is the limiting reactant while P is an excess reagent. After the consumption of all Ca, the remaining P is then available to form AlP, which indicates that fewer nucleation sites (in the form of AlP) are available to nucleate both  $\text{Mg}_2\text{Si}$  and Si. This is fully consistent with our previous work [18,19], where it was assumed that P combines with Ca and forces the formation of eutectic  $\text{Mg}_2\text{Si}$  by supercooling.

The fine fibrous and globular morphology of the Mg<sub>2</sub>Si phase indicates that the formation of AlP compounds may also act as a nuclei for eutectic Mg<sub>2</sub>Si, since physical and structural similarities exist between Mg<sub>2</sub>Si and Si (AlP is a potential substrate for Si) [13,40]. However, it should be noted here that although there are the structural similarities, atomic mismatch between AlP (substrate) and Mg<sub>2</sub>Si (nucleating crystal) is approximately ~14%, which is higher than in the case of AlP for Si. The atomic mismatch between the substrate and nucleating crystals can be calculated through a useful equation proposed by Turnbull [41], as shown below:

$$\delta = \frac{|a_s - a_c|}{a_c} \times 100 \quad (2)$$

where  $a_s$  and  $a_c$  are the lattice parameters of substrate and nucleating crystals. In a deeply etched sample containing 300 ppm P (Figure 9b), a few polygonal-shaped Mg<sub>2</sub>Si particles were observed. The structure consists of squares and hexagons, indicating that it is a geometrical shape identical to a tetrakaidecahedron. This kind of Mg<sub>2</sub>Si morphology was also previously reported by Qin et al. [15] at a very high P content, i.e., 0.41 wt.% P. However, in the present investigation, this morphology was observed at a much lower P content (300 ppm P). Both suggest that at higher levels of P, AlP forms first, which may act as a nucleating agent for primary Mg<sub>2</sub>Si. Due to the fact that no evidence of the attachment of AlP was found, both for eutectic Mg<sub>2</sub>Si and primary Mg<sub>2</sub>Si particles during the TEM investigation, it is therefore impossible to fully clarify the effects of P on the nucleation and growth of the ternary eutectic (Al-Mg<sub>2</sub>Si-Si). A more detailed composition analysis with a higher resolution (i.e., atom probe tomography) is needed. In addition, considering that fact that the spheroidized morphology is effective in enhancing mechanical as well as corrosion properties, further investigations on these properties are also needed.

## 5. Conclusions

We have investigated the effect of Ca and P on the nucleation and growth pattern of eutectic Mg<sub>2</sub>Si in high-purity Al-13.1 wt.% Mg<sub>2</sub>Si near-eutectic alloys without and with the additions of P and Ca. We found that purity levels of the starting materials exert a great influence on the final microstructure of near-eutectic Al-Mg-Si alloys. We proposed that the inherent low levels of Ca, in raw starting materials, promote the faceted growth of Mg<sub>2</sub>Si by forming a Ca-rich layer ahead of the growing fronts. However, at sufficiently higher levels of Ca, it may either substitute inside Mg<sub>2</sub>Si as (Ca, Mg)<sub>2</sub>Si or form Al<sub>2</sub>Si<sub>2</sub>Ca intermetallic. The Al<sub>2</sub>Si<sub>2</sub>Ca intermetallic appears to nucleate on the eutectic Mg<sub>2</sub>Si and forces the Mg<sub>2</sub>Si to grow in the form of blocks and/or plates instead of fibers. P additions suppress the formation of the non-equilibrium ternary eutectic (Al-Mg<sub>2</sub>Si-Si). With the additions of higher levels of P, AlP forms first and acts as a nucleating agent for primary and/or eutectic Mg<sub>2</sub>Si. The present investigation is of great importance for the further development of high-performance Al-Mg<sub>2</sub>Si-based alloys.

**Supplementary Materials:** The following supporting information can be downloaded at: <https://www.mdpi.com/article/10.3390/met13040784/s1>, Equations Supplemental information (SI).

**Author Contributions:** Conceptualization, P.S. and J.L.; methodology, M.Z. and J.L.; formal analysis, J.L.; investigation, M.Z., T.P. and I.S.; resources, P.S.; data curation, J.L.; writing—original draft preparation, M.Z. and J.L.; writing—review and editing, J.L.; supervision, P.S. and J.L.; project administration, P.S. and J.L.; funding acquisition, M.Z. and J.L. All authors have read and agreed to the published version of the manuscript.

**Funding:** This research was funded by Higher Education Commission (HEC) of Pakistan, OEAD and the Austrian Science Fund (FWF), grant number P 32378-N37.

**Data Availability Statement:** The raw/processed data required to reproduce these findings cannot be shared at this time as they also form part of an ongoing study.

**Conflicts of Interest:** The authors declare no conflict of interest. The funders had no role in the design of the study; in the collection, analyses, or interpretation of data; in the writing of the manuscript; or in the decision to publish the results.

## References

1. Hanson, D.; Gayler, M.L.V. The constitution and age-hardening of the alloys of Al with Mg and Si. *J. Inst. Met.* **1921**, *26*, 321–359.
2. Gwyer, A.G.C.; Phillips, H.W.L. Alloys of Aluminium with Silicon and Iron. *J. Inst. Met.* **1927**, *38*, 31–35.
3. Mondolfo, L.F. *Aluminium Alloys: Structure and Properties*, 1st ed.; Butterworth and Co.: London, UK, 1976; p. 787.
4. Davis, J.R. *Aluminium and Aluminium Alloys*, 4th ed.; ASM Specialty Hand Book; ASM International: Novolty, OH, USA, 1998; p. 59.
5. Dix, E.H., Jr.; Keller, F.; Graham, R.W. Equilibrium relations in Aluminum-Magnesium-Silicide alloy of high purity. *Trans. Am. Inst. Min. Metall. Eng.* **1931**, *93*, 404–420.
6. Losana, L. The Ternary System: Aluminium-Magnesium-Silicon. *Metall. Ital.* **1931**, *23*, 367–382.
7. Zhang, J.; Fan, Z.; Wang, Y.Q.; Zhou, B.L. Equilibrium pseudobinary Al–Mg<sub>2</sub>Si phase diagram. *Mater. Sci. Technol.* **2001**, *17*, 494–496. [[CrossRef](#)]
8. Barabash, O.M.; Sulgenko, O.V.; Legkaya, T.N.; Korzhova, N.P. Experimental analysis and thermodynamic calculation of the structural regularities in the fusion diagram of the system of alloys Al–Mg–Si. *JPE* **2001**, *22*, 5–11. [[CrossRef](#)]
9. Li, S.; Zhao, S.; Pan, M.; Zhao, D.; Chen, X.; Barabash, O.M.; Barabash, R.I. Solidification and structural characteristics of  $\alpha$ (Al)–Mg<sub>2</sub>Si eutectic. *Met. Trans. JIM* **1997**, *38*, 553–559. [[CrossRef](#)]
10. Barabash, O.M.; Legkaya, T.N.; Korzhova, N.P.; Sulzhenko, O.V. Thermodynamic Analysis and Experimental Study of Composite Structure Formation in Eutectic Alloys  $\alpha$ -Al + Mg<sub>2</sub>Si. *Powder Metall. Met. Ceram.* **2000**, *39*, 458–461. [[CrossRef](#)]
11. Hanemann, H.; Schrader, A. *Ternäre Legierung des Aluminiums, Atlas Metallographicus, Band III, Teil 2*, 1st ed.; Verlag Stahleisen GmbH: Düsseldorf, Germany, 1952; p. 128.
12. Zhang, J.; Fan, Z.; Wang, Y.Q.; Zhou, B.L. Effect of cooling rate on the microstructure of hypereutectic Al–Mg<sub>2</sub>Si alloys. *J. Mater. Sci. Lett.* **2000**, *19*, 1825–1828. [[CrossRef](#)]
13. Zhang, J.; Fan, Z.; Wang, Y.Q.; Zhou, B.L. Microstructural development of Al–15wt.%Mg<sub>2</sub>Si in situ composite with mischmetal addition. *Mater. Sci. Eng. A* **2000**, *281*, 104–112. [[CrossRef](#)]
14. Zhang, J.; Fan, Z.; Wang, Y.Q.; Zhou, B.L. Microstructure and mechanical properties of in situ Al–Mg<sub>2</sub>Si composites. *J. Mater. Sci. Technol.* **2000**, *16*, 913–918. [[CrossRef](#)]
15. Qin, Q.D.; Zhao, Y.G.; Zhou, W.; Cong, P.J. Effect of phosphorus on microstructure and growth manner of primary Mg<sub>2</sub>Si crystal in Mg<sub>2</sub>Si/Al composite. *Mater. Sci. Eng. A* **2007**, *447*, 186–191. [[CrossRef](#)]
16. Ben-Hamu, G.; Eliezer, D.; Shin, K.S. The role of Mg<sub>2</sub>Si on the corrosion behavior of wrought Mg–Zn–Mn alloy. *Intermetallic* **2008**, *16*, 860–867. [[CrossRef](#)]
17. Li, C.; Liu, X.; Zhang, G. Heterogeneous nucleating role of TiB<sub>2</sub> or AlP/TiB<sub>2</sub> coupled compounds on primary Mg<sub>2</sub>Si in Al–Mg–Si alloys. *Mater. Sci. Eng. A* **2008**, *497*, 432–437. [[CrossRef](#)]
18. Pabel, T.; Schumacher, P. Method for the Refining and Structure Modification of AL-MG-SI Alloys. U.S. Patent No. US9279170B2, 8 March 2016.
19. Pabel, T.; Schumacher, P. Verfahren zur Raffination und Gefügemodifikation von Almg-si-Legierungen. EP Patent No. EP2705171B1, 26 August 2015.
20. Zarif, M.; McKay, B.; Schumacher, P. Study of Heterogeneous Nucleation of Eutectic Si in High-Purity Al–Si Alloys with Sr Addition. *Metall. Mater. Trans. A* **2011**, *42*, 1684–1691. [[CrossRef](#)]
21. Li, J.H.; Zarif, M.Z.; Albu, M.; McKay, B.J.; Hofer, F.; Schumacher, P. Nucleation kinetics of entrained eutectic Si in Al–5Si alloys. *Acta Mater.* **2014**, *72*, 80–98. [[CrossRef](#)]
22. Moussa, M.E.; Waly, M.A.; El-Sheikh, A.M. Effect of Ca addition on modification of primary Mg<sub>2</sub>Si, hardness and wear behavior in Mg<sub>2</sub>Si hypereutectic alloys. *J. Magnes. Alloy* **2014**, *2*, 230–238. [[CrossRef](#)]
23. Shah, A.W.; Ha, S.H.; Kim, B.H.; Yoon, Y.O.; Lim, H.K.; Kim, S.K. Effect of Al<sub>2</sub>Ca addition and heat treatment on the microstructure modification and tensile properties of hypo-eutectic Al–Mg–Si alloys. *Materials* **2021**, *14*, 4588. [[CrossRef](#)]
24. Lotfpoor, M.; Bahmani, A.; Mirzadeh, H.; Emamy, M.; Malekan, M.; Kim, W.J.; Taghizadeh, M.; Afsharnaderi, A. Effect of microalloying by Ca on the microstructure and mechanical properties of as-cast and wrought Mg–Mg<sub>2</sub>Si composites. *Mater. Sci. Eng. A* **2021**, *820*, 141574. [[CrossRef](#)]
25. Vander, G.F. *ASM Handbook Volume 9: Metallography and Microstructures*; ASM International: Novolty, OH, USA, 2004; p. 740.
26. Wang, H.; Davidson, C.J.; St. John, D.H. Semisolid microstructural evolution of AlSi7Mg alloy during partial remelting. *Mater. Sci. Eng. A* **2004**, *368*, 159–167. [[CrossRef](#)]
27. Jung, B.I.; Jung, C.H.; Han, T.K.; Kim, Y.H. Electromagnetic stirring and Sr modification in A356 alloy. *J. Mater. Proc. Technol.* **2001**, *111*, 69–73. [[CrossRef](#)]
28. Lu, S.Z.; Hellawell, A. The mechanism of silicon modification in aluminum-silicon alloys: Impurity induced twinning. *Met. Trans. A* **1987**, *18*, 1721–1733. [[CrossRef](#)]
29. Grobner, J.; Chumak, I.; Schmid-Fetzer, R. Experimental study of ternary Ca–Mg–Si phase equilibria and thermodynamic assessment of Ca–Si and Ca–Mg–Si systems. *Intermetallic* **2003**, *11*, 1065–1074. [[CrossRef](#)]

30. Li, S.P.; Zhao, S.X.; Pan, M.X.; Zhao, D.Q.; Chen, X.C.; Barabash, O.M. Barabash. Eutectic reaction and microstructural characteristics of Al (Li)-Mg<sub>2</sub>Si alloys. *J. Mater. Sci.* **2001**, *36*, 1569–1575. [[CrossRef](#)]
31. Jackson, K.A. Liquid Metal and Solidification. In *Growth and Perfection of Crystals*; Doremus, R.H., Roberts, B.W., Turnbull, D., Eds.; Wiley and Sons: New York, NY, USA; ASM: Cleveland, OH, USA, 1958; p. 319.
32. Rosenqvist, T. *Principles of Extractive Metallurgy*, 2nd ed.; Tapir Academic Press: Trondheim, Norway, 2004; p. 449.
33. Hellawell, A. The Growth and Structure of Eutectics with Silicon and Germanium. *Prog. Mater. Sci.* **1970**, *15*, 3–78. [[CrossRef](#)]
34. Kottcamp, E.H., Jr. *ASM Handbook Volume 3: Alloy Phase Diagrams*, 2nd ed.; ASM International: Novelt, OH, USA, 1992; p. 2121.
35. Nogita, K.; McDonald, S.D.; Tsujimoto, K.; Yasuda, K.; Dahle, A.K. Aluminium phosphide as a eutectic grain nucleus in hypoeutectic Al-Si alloys. *Microscopy* **2004**, *53*, 361–369. [[CrossRef](#)] [[PubMed](#)]
36. Ho, C.R.; Cantor, B. Heterogeneous nucleation of solidification of Si in Al-Si and Al-Si-P alloys. *Acta Metall. Mater.* **1995**, *43*, 3231–3246. [[CrossRef](#)]
37. Crosley, P.B.; Mondolfo, L.F. The Modification of Aluminum-Silicon Alloys. *AFS Trans.* **1966**, *74*, 53–64.
38. Crosley, P.B.; Mondolfo, L.F. The Modification of Aluminum-Silicon Alloys. *Mod. Cast.* **1966**, *49*, 89–100.
39. Schlesinger, M.E. The thermodynamic properties of phosphorus and solid binary phosphides. *Chem. Rev.* **2002**, *102*, 4267–4301. [[CrossRef](#)]
40. Brandes, E.A.; Brook, C.B. *Smithells Metals Reference Book*, 7th ed.; Butterworths-Heinemann: Oxford, UK, 1992; pp. 6–29.
41. Turnbull, D.; Vonnegut, B. Nucleation Catalysis. *Ind. Eng. Chem.* **1952**, *44*, 1292–1298. [[CrossRef](#)]

**Disclaimer/Publisher’s Note:** The statements, opinions and data contained in all publications are solely those of the individual author(s) and contributor(s) and not of MDPI and/or the editor(s). MDPI and/or the editor(s) disclaim responsibility for any injury to people or property resulting from any ideas, methods, instructions or products referred to in the content.